Supplementary information for efficient readout of a single spin state in diamond via spin-to-charge conversion

B. J. Shields,[1] Q. P. Unterreithmeier,[1] N. P. de Leon,[1] H. Park,[2,1] and M. D. Lukin[1]

[1] *Harvard University Physics Department*

[2] *Harvard University Department of Chemistry & Chemical Biology*

(Dated: February 14, 2015)

LIGHT SOURCES

For the SCC readout, we use three different lasers to address different processes in the NV center. First, a 532-nm laser (Coherent Compass 315M) provides light for pumping the NV into the negative charge state. An acousto-optic modulator in double-pass configuration controls the intensity of the 532-nm light. Second, a 594-nm helium neon laser (Thorlabs) provides light to measure the NV charge state, and to shelve $m_s = 1$ into the metastable singlet state. An acousto-optic modulator in single-pass configuration controls the intensity of the 594-nm light. Finally, a diode laser operating at 637-nm (Thorlabs, HL63133DG) provides light to rapidly ionize the NV from the negative to the neutral charge state. The diode is actively cooled to $-9\,^\circ$°C to tune the wavelength to 637-nm in order to match the NV zero phonon line. The 637-nm wavelength was more effective for the ionization step than 594-nm light because it drives the NV^0 transition less efficiently. An acousto-optic modulator in single-pass configuration controls the intensity of the 594-nm light. All lasers are fiber-coupled to the confocal microscope setup, and their timing is controlled by a 500 MHz PulseBlasterESR-PRO (SpinCore).

Additionally, we use a 110 ps, pulsed, 530-nm laser (PicoQuant LDH-P-FA-530L) for lifetime measurements of the NV^- excited state. An acousto-optic modulator in single-pass configuration picks pulses from the pulse train.

DEVICE FABRICATION

We employ an angled RIE fabrication technique[S1] to carve 300 nm-wide, triangular cross-section nanobeams from a bulk diamond sample. To do so, we begin with a polished diamond sample (Element6, type IIa, 1ppm N concentration) and remove ~ 600 nm of material from the top surface in a top-down oxygen RIE step. Next, we spin a PMMA layer onto the diamond and pattern the beam mask shape via e-beam lithography. After developing the PMMA, a 294 nm-thick layer of Al_2O_3 is sputtered and the PMMA is stripped, transferring the etch mask pattern into the Al_2O_3 layer. Next, we perform a top-down etch for 3 min in O_2 plasma to create vertical clearance for the angled etch. Following the top-down etch, the angled etch is performed in a Faraday cage with sloped mesh walls for a total of 7 min in O_2 + Cl_2 plasma, with the etch broken into 12 cycles of 35 s each. The diamond is then cleaned in a boiling solution of 1:1:1 perchloric, nitric, and sulfuric acids, and annealed in a 3-stage ramp consisting of 3 h ramp from room temperature to 400 °C, annealing at 400 °C for 4 h, 3 h ramp from 400 °C to 800 °C, annealing at 800 °C for 8 h, 12 h ramp from 800 °C to 1200 °C, anneal at 1200 °C for 2 h, ramp down to room temperature. Following the anneal the diamond is again acid cleaned and baked at 465 °C in oxygen environment.

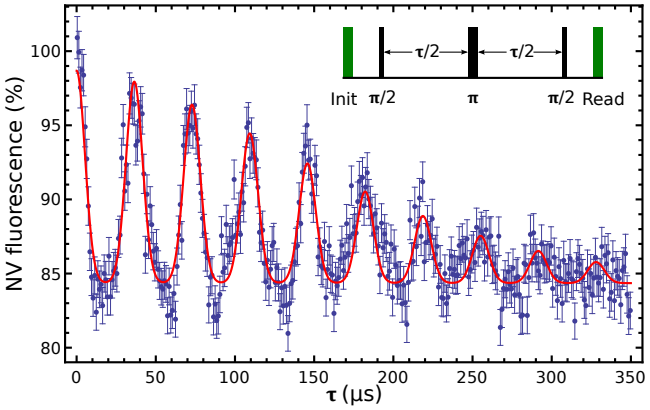

Figure S1. Spin echo for NV in nanobeam. The blue points are fluorescence measured after a Hahn echo, normalized to the fluorescence level with no echo pulses. The red curve is a fit to the data (see text).

NV SPIN COHERENCE

We observe similar spin coherence properties in the nanobeams as in bulk, natural ^{13}C abundance diamond[S2]. A Hahn echo measurement is shown in Fig. S1 for a similarly prepared beam as that used for the SCC measurements. The data is fitted by the function[S2]:

$$F(\tau) = A + Be^{-(\tau/T_2)^n} \sum_{j=0}^{9} e^{-((\tau - jT_{rev})/T_{dec})^2}, \quad \text{(S1)}$$

with $A = 0.844 \pm 0.001$, $B = 0.143 \pm 0.005$, $n = 1.72 \pm 0.14$, $T_{rev} = 36.48 \pm 0.04\mu$s, $T_{dec} = 7.47 \pm 0.22\mu$s, and

$T_2 = 201 \pm 7\mu$s.

MODEL FOR PHOTON STATISTICS

To characterize the charge state quantitatively, we assumed that the dynamics can be fully described by 4 rates: the ionization rates from NV^- to NV^0 and vice versa (g_{-0} and g_{0-}, respectively), and the photon count rates when in NV^- and NV^0 (γ_1 and γ_0, respectively). From $\gamma_{1,0}$, we can calculate the photon number distribution that results from a particular sequence of ionization events. For example, suppose the NV begins in NV^-, jumps to NV^0 after time τ_1, then jumps back to NV^- after an additional time t_1 and remains in NV^- for the rest of the counting window. The photon number distribution for that ionization sequence would be a Poisson distribution with mean value $\gamma_1(t_R - t_1) + \gamma_0 t_1$. The total photon number distribution for a particular initial charge state and total counting time t_R is then a sum over the photon number distributions for all possible ionization sequences, weighted by the probability for each sequence to occur. In the case that the initial state is NV^-, we have:

$$p(n|\mathrm{NV}^-,\mathrm{odd}) = \int_0^{t_R} d\tau e^{(g_{0-}-g_{-0})\tau - g_{0-}t_R} \sum_{i=1}^{\infty} g_{-0}^{i} g_{0-}^{i-1} \prod_{j=1}^{i-1} \int_0^{\tau - \sum_{k=1}^{(j-1)} \tau_k} ds_j \times \prod_{j=1}^{i-1} \int_0^{(t_R-\tau) - \sum_{k=1}^{(j-1)} t_k} dt_j \mathrm{PoissPDF}(\gamma_1\tau + \gamma_0(t_R-\tau), n) \quad \text{(S2)}$$

$$p(n|\mathrm{NV}^-,\mathrm{even}) = \int_0^{t_R} d\tau e^{(g_{0-}-g_{-0})\tau - g_{0-}t_R} \sum_{i=1}^{\infty} (g_{-0}g_{0-})^{i} \prod_{j=1}^{i} \int_0^{\tau - \sum_{k=1}^{(j-1)} \tau_k} d\tau_j \times \prod_{j=1}^{i-1} \int_0^{(t_R-\tau) - \sum_{k=1}^{(j-1)} t_k} dt_j \mathrm{PoissPDF}(\gamma_1\tau + \gamma_0(t_R-\tau), n) + e^{-g_{-0}t_R} \mathrm{PoissPDF}(\gamma_1 t_R, n) \quad \text{(S3)}$$

where τ is the total time spent in NV^- and must therefore be integrated over $[0, t_R]$, $\mathrm{PoissPDF}(x, n)$ is the probability distribution function for an outcome of n for a Poisson random variable with mean value x, and we have broken the result into those cases where there are an odd total number of ionization events and an even number. The last term in the expression for $p(n|\mathrm{NV}^-, \mathrm{even})$ is the zero ionization event case. For the case of NV^0 as the initial state, simply exchange $1 \leftrightarrow 0$. The integral products can be evaluated as the volume of a pyramid in i dimensions, and consequently the sum over ionization events reduces to an expression in terms of Bessel functions:

$$p(n|\mathrm{NV}^-,\mathrm{odd}) = \int_0^{t_R} d\tau g_{-0} e^{(g_{0-}-g_{-0})\tau - g_{0-}t_R} \mathrm{BesselI}(0, 2\sqrt{g_{-0}g_{0-}\tau(t_R-\tau)}) \mathrm{PoissPDF}(\gamma_1\tau + \gamma_0(t_R-\tau), n) \quad \text{(S4)}$$

$$p(n|\mathrm{NV}^-,\mathrm{even}) = \int_0^{t_R} d\tau \sqrt{\frac{g_{-0}g_{0-}\tau}{t_R-\tau}} e^{(g_{0-}-g_{-0})\tau - g_{0-}t_R} \mathrm{BesselI}(1, 2\sqrt{g_{-0}g_{0-}\tau(t_R-\tau)}) \mathrm{PoissPDF}(\gamma_1\tau + \gamma_0(t_R-\tau), n) + e^{-g_{-0}t_R} \mathrm{PoissPDF}(\gamma_1 t_R, n), \quad \text{(S5)}$$

where $\mathrm{BesselI}(m, x)$ is a modified Bessel function of the first kind. To evaluate these photon number distributions, we performed the integral numerically in *Mathematica*. This model accurately captures the behavior of the system under the cw, low power illumination conditions used for charge readout, as shown in Fig. S2

MEASURING IONIZATION AND PHOTON COUNT RATES

The above model can be used to find the ideal power and time settings that maximize $\mathcal{F}_C$, once the ionization and photon count rates are known. To measure these, we integrated the counts over a time window $t_R \sim 1/g_{-0}(P)$ for a range of cw 594-nm powers, P, and used the model

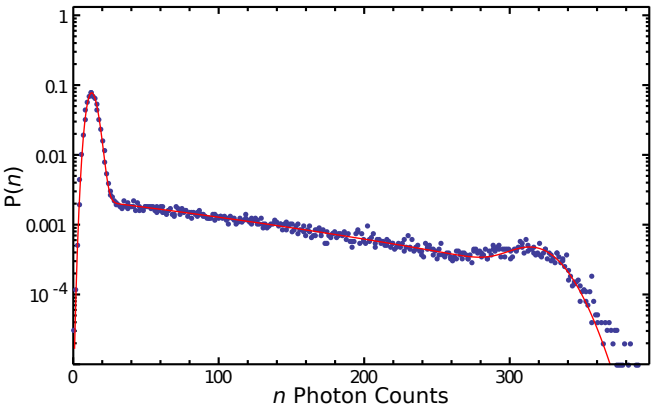

Figure S2. Example of model for photon statistics. Data was taken under 875 nW illumination with cw 594-nm light, integration time 8 ms. 100,000 measurements.

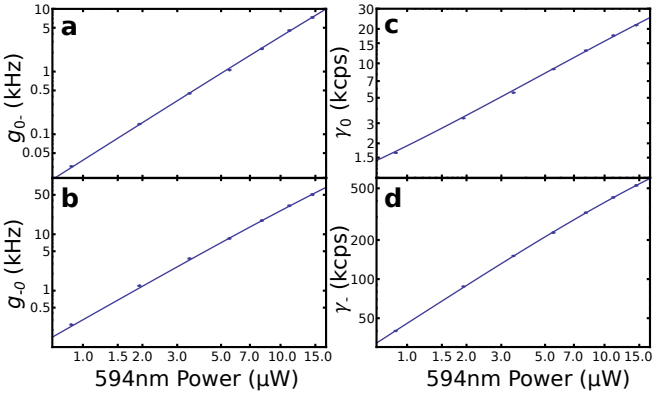

Figure S3. Ionization and photon count rates under cw 594-nm illumination. (a) g_{0-}, fitted with a model of the form $aP^2/(1+P/P_{sat})$ with $P_{sat} = 134\,\mu$W, $a = 39$ cps/μW^2. (b) g_{-0}, fitted with a model of the form $aP^2/(1+P/P_{sat})$ with $P_{sat} = 53.2\,\mu$W, $a = 310$ cps/μW^2. (c) γ_0, fitted with a model of the form $a*P/(1+P/P_{sat})+dc$, with detector dark count rate $dc = 0.268$ kcps measured independently, $a = 1.65$ kcps/μW, $P_{sat} = 134\,\mu$W. (d) γ_1, fitted with a model of the form $a*P/(1+P/P_{sat})+dc$, with $a = 46.2$ kcps/μW, $P_{sat} = 53\,\mu$W. 100,000 measurements were taken at all power levels. Saturation power levels were determined from fits to the $\gamma_{0,1}$ data and the fitted values were then used for the fits of $g_{0-,-0}$.

to fit the photon number distribution from 100,000 measurements. The choice of t_R is made to ensure that sufficient ionization events occur to get an accurate fit of the ionization rates. Since the measurement was steady state, it is sufficient to select t_R to be long enough to measure g_{-0}, since $g_{0-,-0}$ are related by the steady state population balance: $g_{0-}/g_{-0} = p(NV^-)/p(NV^0)$.

The rates measured via the above fitting procedure for cw 594-nm powers from 875 nW to 14.5 μW are shown in Fig. S3 (blue points). The count rates are fitted by an expression of the form $a*P/(1+P/P_{sat})+dc$ where P_{sat} is the saturation power and dc is the detector dark count

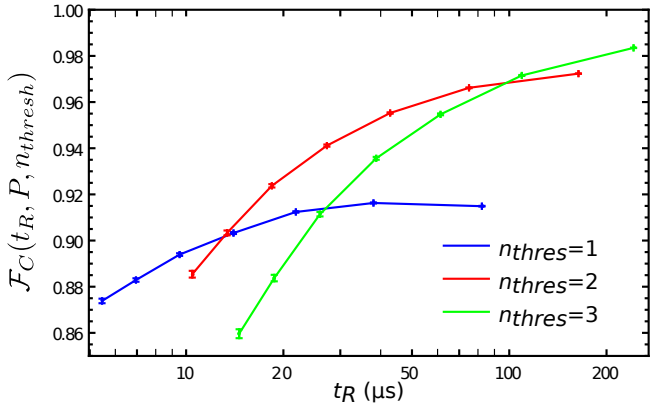

Figure S4. Calculated optimal $\mathcal{F}_C$ for a range of powers at photon thresholds $n_{thresh} = [1, 2, 3]$. For each power and threshold combination, the readout time is optimized to maximize $\mathcal{F}_C$.

rate, measured to be 0.268 kcps. The ionization rates are fitted by an expression of the form $aP^2/(1+P/P_{sat})$, where P_{sat} is taken from the corresponding photon count rate fit.

Having measured the rates, we proceed to determine the optimal readout times and corresponding $\mathcal{F}_C(P, t_R)$ for the set of 594-nm powers used. To do so, we use a simple thresholding algorithm ($n \geq n_{thresh} \rightarrow NV^-$, $n < n_{thresh} \rightarrow NV^0$) under the assumption of a 50/50 charge state population balance. Then, using the photon distribution from the above model, we calculate the probability of correctly determining the charge state, and maximize that outcome with respect to t_R for each power, using a photon threshold of $n_{thresh} = [1, 2, 3]$. The resulting 3 data sets (one for each photon threshold) are shown in Fig. S4. We use the optimal threshold at each value of t_R for the plot in Fig. 2b.

READOUT NOISE AND MAGNETOMETER SENSITIVITY

We consider the following scheme for sensing AC magnetic fields with an NV:

1. initialize the NV into $|m_s = 0\rangle$, in time t_I,
2. carry out a Hahn echo pulse sequence occupying time τ,
3. read out the NV spin, in time t_R.

At the end of the echo sequence, the state of the system is

$$|\psi(\tau)\rangle = \cos\left(\frac{g\mu_B B\tau}{\pi\hbar}\right)|\mathrm{m_s}=0\rangle - i\sin\left(\frac{g\mu_B B\tau}{\pi\hbar}\right)|\mathrm{m_s}=1\rangle, \quad \text{(S6)}$$

where g is the electron Landé g factor and B is the magnitude of the magnetic field. The measurement procedure projects onto one or another of $|\mathrm{m_s}=0\rangle, |\mathrm{m_s}=1\rangle$, with probabilities:

$$p_0 = \cos^2\left(\frac{g\mu_B B\tau}{\pi\hbar}\right) \tag{S7}$$

$$p_1 = 1 - p_0 = \sin^2\left(\frac{g\mu_B B\tau}{\pi\hbar}\right). \tag{S8}$$

During the measurement, we count the number of photons collected from the NV and assign the result to either NV^- or NV^0. For the two spin states, we denote the probabilities of measuring NV^- as $\tilde{\beta}_0$ and $\tilde{\beta}_1$. For a perfect charge state, $\tilde{\beta}_i = \beta_i$. The signal S that we record is the fraction of repetitions of the experiment for which the result is NV^-. The expected signal for a measurement of the superposition state $|\psi(\tau)\rangle$ (eq. S6) will be:

$$S = p_0\tilde{\beta}_0 + p_1\tilde{\beta}_1. \tag{S9}$$

The minimum detectable change in the magnitude of the magnetic field, δB, is that which shifts the mean $\langle S\rangle$, by the width, σ_S:

$$\delta B = \frac{\sigma_S}{\partial\langle S\rangle/\partial B} = \frac{\pi\hbar}{g\mu_B\tau}\frac{\sigma_S}{\tilde{\beta}_0 - \tilde{\beta}_1}, \tag{S10}$$

where we have taken $p_0 = p_1 = 1/2$, to maximize the slope of the signal with respect to a change in magnetic field amplitude. The sensitivity is related to δB by the square root measurement time. Thus:

$$\eta = \delta B\sqrt{\tau + t_I + t_R} = \frac{\pi\hbar}{2g\mu_B} \times \sigma_R \times \sqrt{\frac{\tau + t_I + t_R}{\tau^2}}. \tag{S11}$$

where we have defined $\sigma_R = \frac{2g\mu_B\tau}{\pi\hbar}\frac{\sigma_S}{\partial S/\partial B}$ to be the readout noise per shot, normalized so that for a measurement where spin projection noise is the only source of uncertainty, $\sigma_R = 1$. In general, σ_R will be a function of t_I and t_R, so that improvements in σ_R must be balanced with the associated requirements in overhead time.

We now derive an expression for σ_R in the case of spin readout based on the SCC mechanism. Recall that we consider operation at the point $p_0 = p_1 = 1/2$:

$$\sigma_R^{SCC} = \frac{2g\mu_B\tau}{\pi\hbar}\frac{\sigma_S}{\partial\langle S\rangle/\partial B} \tag{S12}$$

$$\langle S\rangle = p_0\beta_0 + (1-p_0)\beta_1 \tag{S13}$$

$$\frac{\partial\langle S\rangle}{\partial B} = \frac{g\mu_B\tau}{\pi\hbar}(\beta_0 - \beta_1) \tag{S14}$$

$$\sigma_S^2 = \frac{\tilde{\beta}_0 + \tilde{\beta}_1}{2} - \langle S\rangle^2 = \frac{1}{2}(\tilde{\beta}_0 + \tilde{\beta}_1) - \frac{1}{4}(\tilde{\beta}_0 + \tilde{\beta}_1)^2$$
$$= \frac{1}{4}(\tilde{\beta}_0 + \tilde{\beta}_1)(2 - \tilde{\beta}_0 - \tilde{\beta}_1) \tag{S15}$$

$$\sigma_R^{SCC} = \sqrt{\frac{(\tilde{\beta}_0 + \tilde{\beta}_1)(2 - \tilde{\beta}_0 - \tilde{\beta}_1)}{(\tilde{\beta}_0 - \tilde{\beta}_1)^2}} \tag{S16}$$

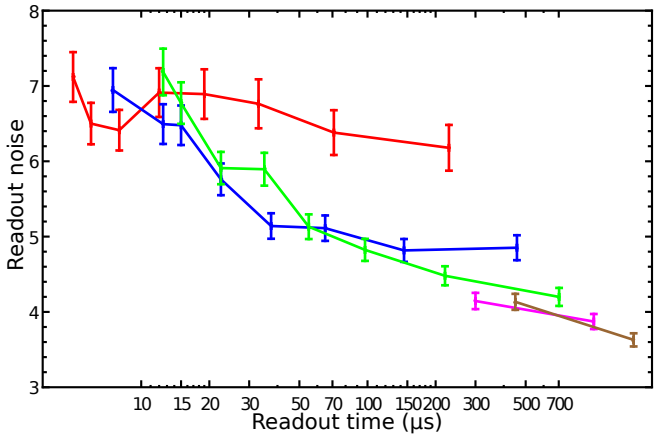

Figure S5. Measured values of σ_R^{SCC} for a set of powers and times chosen to optimize the readout noise for a photon threshold of 1 photon (red points), 2 photons (blue points), 3 photons (green points), 4 photons (magenta points), or 6 photons (brown points).

MEASURING READOUT NOISE VS. READOUT TIME

We measured $\tilde{\beta}_{0,1}$ for a range of readout powers. For each power, we measured the ionization and photon count rates, and optimized the readout time to minimize σ_R^{SCC} for the set of threshold photon numbers $n_{thresh} = \{1,2,3,4,6\}$ (for $n_{thresh} = \{4,6\}$ we only used the two lowest powers). For each (power, time, threshold) combination, we ran the SCC sequence after a fast initialization and iterated 100,000 times. The results of all measurements are shown in Fig. S5. As with the measurement of $\mathcal{F}_C(t_R)$, we used each photon number threshold in its optimal range for the plot in Fig. 4.

In order to estimate the magnetometer sensitivity from this measurement, we need an approximate functional dependence for $\sigma_R^{SCC}(t_R)$, valid over the measurement range. We used a fit function of the form $f(t_R) = 1 + at_R^{-b}$, with fitting parameter values $a = 7.54$, $b = 0.146$. The projected η for a given τ is found by minimizing $f(t_R)\sqrt{t_I + t_R + \tau}$ with respect to t_R.

INITIAL SPIN POLARIZATION

The measurements of σ_R^{SCC} all include the effect of imperfect spin polarization. Upon excitation, an initial NV^- state of $m_s = 1$ is excited and decays preferentially into the singlet state, where it can decay back to $m_s = 0$ or $m_s = 1$. The limited branching ratios at each decay step result in imperfect spin polarization. To measure the electron spin polarization of the NV, we perform measurement of the triplet excited state lifetime as the NV undergoes Rabi nutations in the ground state[S3]. We use the pump-probe sequence (150 ns, 300 µW, 532-

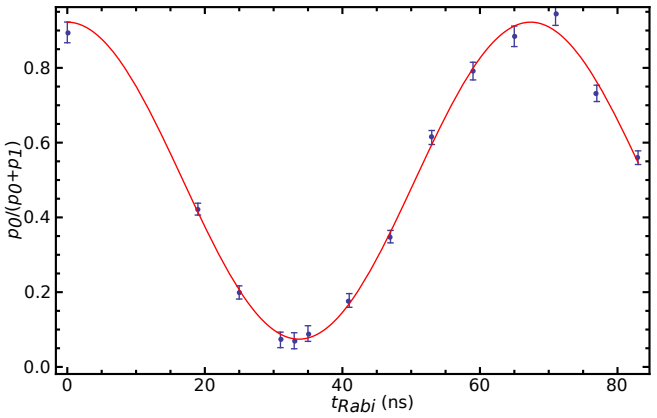

Figure S6. Initial spin polarization. The NV is initialized with a pump-probe sequence, then a microwave pulse of duration t_{Rabi} rotates the spin into a superposition of $m_s = 0$ and $m_s = 1$, and the fluorescence decay is recorded upon excitation with a 110 ps pulsed source. From the decay, the population in $m_s = 0$ is extracted (blue points) and fitted by a sinusoid (red curve) to find the initial spin polarization.

nm pump pulse followed by a 200 ns delay and then the 900 ns, 11 µW 594-nm probe pulse) to initialize the center into NV^-. Then, after a 3 µs delay, we apply a microwave pulse of duration t_{Rabi} followed by a 2 µs delay and a 110 ps pulse of 530-nm light, set to low power to avoid any effect of ionization from this pulse. This measurement sequence is repeated every 9 µs for 600 s. The fluorescence intensity $I(t)$ subsequent to the 110 ps pulse is recorded with a time-correlated single photon counting module (PicoHarp 300, PicoQuant) and conditioned on detection of a probe photon (this selection is carried out in post processing). This results in ∼75,000 fluorescence lifetime photons for each value of t_{Rabi}. We fit this fluorescence decay by a sum of two exponentially modified Gaussian distributions:

$$I(t) = p_0(t_{Rabi})F(t,\tau_0) + p_1(t_{Rabi})F(t,\tau_1) + c. \quad \text{(S17)}$$

Here, p_0 and p_1 are the amplitude in $m_s = 0$ and $m_s = 1$, t is the delay after the 110 ps pulse, and $F(t,\tau)$ is an exponentially modified Gaussian with exponential decay constant τ. The decay constants were found to be $\tau_0 = 18.2$ ns and $\tau_1 = 7.9$ ns. We find the fraction of population in $m_s = 0$ for each value of t_{Rabi} (blue points in Fig. S6) and fit the result with the function:

$$p_0(t_{Rabi}) = a\cos(\omega t_{Rabi}) + c, \quad \text{(S18)}$$

with $a = 0.42 \pm 0.01$ and $c = 0.50 \pm 0.01$, so that the initial polarization is $p_0(0) = 0.92 \pm 0.01$.

[S1] M. J. Burek, N. P. de Leon, B. J. Shields, B. J. M. Hausmann, Y. Chu, Q. Quan, A. S. Zibrov, H. Park, M. D. Lukin, and M. Lončar, Nano Letters **12**, 6084 (2012).

[S2] L. Childress, M. V. Gurudev Dutt, J. M. Taylor, A. S. Zibrov, F. Jelezko, J. Wrachtrup, P. R. Hemmer, and M. D. Lukin, Science **314**, 281 (2006).

[S3] L. Robledo, H. Bernien, T. van der Sar, and R. Hanson, New Journal of Physics **13**, 025013 (2011).